

1 **BEHAVIOR OF EPOXY BONDED BARS IN CONCRETE AFFECTED BY**
2 **ALKALI-SILICA REACTION**

3 Félix-Antoine Villemure, Mathieu Fiset, Josée Bastien, Denis Mitchell and Benoit Fournier

4 **Biography:**

5 **Félix-Antoine Villemure** is a M. Sc. candidate in the Department of Civil Engineering at
6 Université Laval, Quebec City, Canada. He received his B. Eng. degree from Université Laval. He
7 is also working as a structural engineer at WSP Canada in Quebec City, Canada. His research
8 interests include materials engineering, concrete durability, structures strengthening and bond
9 behavior in reinforced concrete structures.

10 **Mathieu Fiset** is an Assistant Professor in the Department of Applied Science at University of
11 Québec in Chicoutimi, Saguenay, Canada. His research interests include structural behavior, shear
12 strengthening and bond behavior in reinforced concrete structures.

13 **Josée Bastien** is a Professor in the Department of Civil and Water Engineering of Université
14 Laval and Presidium member of the International Federation of Structural Concrete (*fib*). Her
15 research interests include the various aspects of design, condition assessment, and sustainability of
16 bridge structures.

17 ACI member **Denis Mitchell**, FACI, is a Professor in the Department of Civil Engineering and
18 Applied Mechanics at McGill University. He is a member of ACI Committees 408, Bond and
19 Development of Reinforcement and Joint ACI-ASCE Committee 445, Shear and Torsion. His
20 research interests include shear behavior, seismic design, the use of high-performance concrete
21 and failure investigations.

22 ACI member **Benoit Fournier** is a Professor in the Department of Geology and Geological
23 Engineering at Université Laval, Quebec City, QC, Canada. His research interests include the
24 various aspects of aggregates technology, recycling and sustainable development in concrete

25 construction, and durability of concrete, especially concrete incorporating supplementary
26 cementitious materials.

27 **ABSTRACT**

28 Installation of drilled-in epoxy bonded reinforcing bars is generally an effective strengthening
29 method to increase the flexural and shear capacities of deficient concrete structures. However,
30 most of the available studies characterizing the bond behavior of epoxy bonded bars in concrete
31 have been carried out on sound concrete elements, i.e., without any pathological material damage.
32 This raises the question of bond capacities in existing damaged elements. This study investigates
33 the influence of alkali-silica reaction (ASR) on the capacity of post-installed reinforcing bars.
34 ASR is a deleterious mechanism that causes expansion and cracking in the affected concrete
35 elements. Pull-out tests on post-installed reinforcing bars having embedded lengths of $2d_b$, $4d_b$ and
36 $5d_b$ with 15M reinforcing bars ($d_b = 15.9$ mm [0.626 in]) have demonstrated a drop in bond
37 strength when concrete is affected by ASR. In addition, the study revealed that the progression of
38 concrete expansion due to ASR, may lead to some confinement of the post-installed reinforcing
39 bar and possible increases the bond strength.

40 **Keywords:** post-installed reinforcing bar; pullout test; alkali-silica reaction (ASR); bond

41 **INTRODUCTION**

42 Many older thick concrete slabs were designed with the shear carried by the concrete, without any
43 shear reinforcement. However, shear failures in structures without shear reinforcement are very
44 brittle. This type of failure occurs with little or no warning signs and a low deformation capacity
45 that limits the redistribution of the internal shear stresses in the structure. The collapse of the
46 Concorde overpass on September 30th, 2006 in Laval (Canada), after 36 years in service,
47 demonstrates the hazardousness and the brittleness of shear failures in aging thick concrete

48 members without shear reinforcement¹. This event demonstrated that degradation of the concrete
49 material may reduce the concrete shear capacity. Moreover, increased traffic loads compared to
50 the loading considered at the time of the design reduces the safety of such structures. Similar
51 structures built between the 50's and 70's in Canada now show signs of concrete degradation and
52 some of them required shear strengthening.

53 Several shear strengthening techniques for existing thick concrete slabs were investigated in the
54 past few years. Tests indicated that one of the most efficient strengthening methods consists of
55 inserting vertical shear reinforcing bars in pre-drilled holes, anchored with epoxy adhesive^{2,3} (see
56 Fig. 1). This technique also proved to be efficient in slabs to resist punching⁴ and for beam-to-
57 column connections⁵. Results indicated that the bond behavior of post-installed bonded shear
58 reinforcement appeared to be the most important parameter governing the shear reinforcement
59 efficiency. The intersection of the critical shear crack with the post-installed bonded bars
60 determines the bar embedded lengths above the crack intersection and below the crack
61 intersection. The bond-slip relationship dictates the ability of the added bars to develop tensile
62 stresses and hence influences the shear contribution of the shear reinforcement, as well as the
63 crack width which, in turn, influences the aggregate interlock and thus, the shear capacity
64 provided by the concrete^{6,7}.

65 The bond-slip relationship of an embedded bar is governed by three principal bond force transfer
66 mechanisms: chemical adhesion along surfaces (bar and/or concrete) as well as friction, and
67 bearing on the bar ribs^{8,9}. On the contrary to cast-in-place bars, post-installed bonded bars are
68 composed of two different interfaces: bar to bonding material (grout, epoxy, etc.) and bonding
69 material to concrete. The chemical adhesion and the friction mechanisms are influenced by the
70 installation conditions, i.e., the surface roughness and the presence of dust or any other
71 contaminant on the bars and/or concrete surfaces. For cast-in-place bars, the bearing capacity

72 depends on the concrete mechanical properties and on the bar geometry, i.e., the rib bearing area
73 and the spacing between ribs along the bar ¹⁰⁻¹⁷. The capacity of post-installed reinforcing bars
74 also depends on the bonding material properties. The effect of cracks on the response of bonded
75 anchors and post-installed reinforcing bars have been investigated ^{5, 16}. It was observed that
76 concrete cracks parallel to the anchors influence bond strength. In his researches, Mahrenholtz⁵
77 observed a large scatter in the bond strength in cracked specimens due to the influence of the bars
78 post-installation conditions. According to Eligehausen & *al.*¹⁶, the bond strength loss due to the
79 propagation of mechanical cracking on post installed reinforcing bars can be considered as 50% of
80 the typical bond strength of post-installed reinforcing bars in sound concrete. The cracking pattern
81 studied was one single crack crossing the bar. Although some bond slip relationships are available
82 in the literature for cast-in-place or post-installed epoxy bonded bars ^{16, 18, 19} these are based on
83 experimental studies performed on sound concrete elements. In the context of shear strengthening
84 of existing concrete structures, it is expected that concrete may have experienced damage and
85 cracking that may originate from many different phenomena such as loading cycles, freeze-thaw
86 cycles, steel corrosion and alkali-silica reaction (ASR) to name a few.

87 Among these, ASR is a very common deleterious mechanism resulting from the chemical reaction
88 between the alkali hydroxide ions (K^+ , $Na^+ - OH^-$) within the pore solution of concrete and some
89 siliceous mineral phases from the fine and/or the coarse aggregates. ASR generates a hygroscopic
90 alkali-silica gel inside the reactive aggregates that swells under high relative humidity conditions,
91 leading to the formation of cracks in the aggregate particles and, eventually, extending into the
92 cementitious matrix. The cement dosage, the use of de-icing salts and the exposure to sea water
93 represent examples of alkali sources which may be significant in existing bridges and influencing
94 the reaction kinetic and longevity. Amongst other parameters, the ASR potential and reaction
95 kinetics of aggregate materials will depend on the nature and proportion of the siliceous phase

96 within the reactive rock types, as well as the aggregate particle size, the ASR potential is
97 influenced by the specific area of the silica particles, i.e., the reaction tends to occur more rapidly
98 as the fineness of particles decreases²⁰. Deleterious effects on ASR-affected structures will last as
99 long as the favorable conditions, i.e., pH over 13, high amount of alkali, unstable siliceous
100 material and high relative humidity, are maintained. Research on the effects of ASR in concrete is
101 given by Sims & *al.*²¹, Lindgård & *al.*²⁰, Sanchez & *al.*²², Thomas & *al.*²³ and Hobbs²⁴. Many
102 authors have demonstrated that the material mechanical properties decrease for affected concrete
103 specimens/elements^{22, 25-28}. Since ASR is very common in North America, this paper aims to
104 investigate its effect on bond strength of post-installed reinforcement.

105 RESEARCH SIGNIFICANCE

106 Since many damaged existing structures are in need of shear strengthening, the effect of a
107 damaged concrete matrix on the bond mechanical properties of post-installed reinforcing bars
108 must be better understood. This research compares the bond mechanical properties of epoxy
109 bonded bars embedded in sound concrete to the ones in concrete affected by alkali-silica reaction
110 (ASR) through pullout tests. Moreover, the effects of ASR progression on the bond strength of an
111 already existing post-installed reinforcing bar were studied.

112 EXPERIMENTAL INVESTIGATION

113 The pullout tests were performed on sound and ASR-damaged concrete. The following paragraphs
114 describe the concrete mixes, specimen geometry as well as testing procedure.

115 Concrete Materials

116 Concrete mixes were designed in order to reach 35 MPa (5000 psi) of compressive strength after
117 28 days of moist curing. A highly reactive coarse aggregate (high amount of reactive silica
118 particles) from Albuquerque (New Mexico) and a high-alkali Portland cement ($\text{Na}_2\text{O}_{\text{eq}}$ of 1.12%)
119 were selected in order to accelerate the development of ASR. Tests carried-out by Sanchez²⁹ and

120 Villeneuve³⁰ confirm the coarse aggregate reactivity. The petrographic facies and potentially
121 reactive phases of the New Mexico (NM) aggregate are presented in Table 1³⁰. NaOH was added
122 to the reactive concrete mix to accelerate the ASR reaction. The final mix design had a $\text{Na}_2\text{O}_{\text{eq}}$
123 content of 1.25% per mass of cement, which is sufficient to allow ASR with the extremely
124 reactive NM aggregate²⁴. Based on the same concrete mix design, a sound concrete mix was
125 produced by incorporating a lithium nitrate (LiNO_3 – 30% solid; lithium-to-alkali molar ratio of
126 0.93 calculated in accordance with Thomas & *al.*³¹ admixture to inhibit the ASR. Non-reactive
127 granitic sand from Quebec City was included in the two concrete mixes. Their water-to-cement
128 ratio is 0.47. The two concrete mix designs are presented in Table 2.

129 **Specimens**

130 Twenty four (24) concrete blocks, 350 x 350 x 350 mm (13.78 x 13.78 x 13.78 in) in size, were
131 cast. These geometrical dimensions were chosen to avoid concrete splitting during testing. Twelve
132 (12) specimens of ASR reactive concrete (specimens A) and twelve (12) other companion
133 specimens of sound concrete (specimens S) were cast. All these specimens were cured and
134 conditioned under the same environmental conditions.

135 After 28 days of moist curing at room temperature ($23 \pm 2^\circ\text{C}$ [$73.4 \pm 3.6^\circ\text{F}$]), test specimens type
136 S and type A were stored in hermetic containers, in a room at 38°C (100.4°F). Relative humidity
137 inside the containers was kept over 95% during conditioning. The expansion caused by ASR was
138 monitored according to embedded stainless steel stud's relative displacements on three faces of
139 the concrete cubes. Dimensional changes parallel and perpendicular to the casting plane (Fig. 2)
140 were monitored separately.

141 Two series of pullout tests were carried out. For the first series, specimens A1 and S1 were tested
142 when the perpendicular expansions of specimens A1 have reached 0.20% in average (~100 days).
143 For the second series, specimens A2 and S2 were tested when the perpendicular expansions of
144 specimens A2 have reached 0.30% in average (~200 days).

145 Following the conditioning period, holes were drilled with a percussion drill into the concrete
146 specimens and cleaned according to the manufacturer specifications. Epoxy adhesive (see Table 3
147 for the mechanical properties of epoxy) was injected into the concrete holes and steel reinforcing
148 bars (cross section area $A_b = 200 \text{ mm}^2$ [0.310 in²] and diameter $d_b = 15.9 \text{ mm}$ [0.626 in]) were
149 installed according to three different embedded lengths (h_{eff}) of $2d_b$, $4d_b$ and $5d_b$ (~32 mm [1.26
150 in], 64 mm [2.52 in] and 80 mm [3.15 in]). The rib index F_R of the reinforcing bars, which is
151 defined by the average rib height (1.2 mm, 0.047 in) divided by the average rib spacing (9.7 mm,
152 0.382 in), was 0.125 satisfying ASTM-A996/A996M³² requirements. The post-installed
153 reinforcing bars were installed so that their longitudinal axis was perpendicular to the concrete
154 casting plane. The selected bar diameter is the same as the one considered for post-installed shear
155 reinforcement in previous concrete thick slab tests ^{2,3}.

156 Some of the concrete blocks were used twice as one bar was installed on two opposite sides of the
157 same concrete specimen making sure that these two bars would not disturb one another's behavior
158 under pullout testing. Finally, two specimens type A1 and two specimens type A2 were used in a
159 third series to study the effects of further ASR damage progression on the bond behavior of
160 already installed bars. These specimens, identified as D1 and D2, are based on specimens A1 and
161 specimens A2, respectively, who were returned to conditioning and monitored for an
162 approximately additional 100 days after the installation of the bonded bars. It is worth
163 mentioning that the exposed steel bars in these specimens were protected against corrosion with a
164 specialized paint.

165 **Testing Procedure**

166 The test setup designed is shown in Fig. 3. The tension load was applied through the reinforcing
167 bar at a rate of 2 mm/min (0.75 in/min) and the tested specimen concrete block upper face offered
168 bearing capacity with the help of a supporting plate and steel rods. A ball joint was used to ensure
169 proper uniaxial tensile loading. This design was chosen to better control the failure mode, i.e., to

170 avoid concrete cover splitting or concrete cone failure, and to determine the full bond-slip
171 relationship of a pulled out bar. Fig. 3 also shows that the steel reinforcing bar is not bonded to
172 concrete along the top 100 mm (3.94 in) of embedment. That design reduces the effect of
173 confining pressure caused by the top supporting plate^{33,34}. The elongation of the steel reinforcing
174 bars was monitored by two extensometers (unbonded length) while the relative displacement
175 between concrete surface and the steel reinforcing bars (slip s) was monitored by four linear
176 variable differential transformers (LVDTs). After each test, the bar was extracted from the block,
177 the embedded length was precisely measured and pictures of the bar and the concrete block were
178 taken.

179 **ASR Damage Assessment**

180 ASR concrete damage was assessed through the stiffness damage test (SDT)³⁵ and the concrete
181 mechanical properties were determined according to the compressive strength test³⁶, the splitting
182 tensile strength test³⁷ and the Young's modulus test³⁸. These tests were performed on concrete
183 cores (100 X 200 mm [3.94 X 7.87 in]) extracted perpendicularly to the concrete casting plane
184 from the tested specimens. Five (5) compressive loading-unloading cycles were performed on
185 selected concrete cores to assess the degree of damage in ASR affected concrete. Young's
186 modulus (E_c) and stiffness damage index (SDI) were determined based on the SDT results. SDI is
187 a diagnosis parameter defined as the irreversible deformation energy divided by SDT total energy
188 (elastic and irreversible)³⁹. As explained by Allard & al.⁴⁰, the SDI, provides information
189 regarding the level of internal cracking. The Young's modulus was determined as the average
190 from the second and the third loading cycles of the SDT test. In accordance with the SDT
191 procedure proposed by Sanchez & al.³⁹, the maximum stress reached during the SDT test
192 corresponded to 40% of the compressive strength of the sound concrete.

193

MATERIAL RESULTS AND DISCUSSION

194 The following section presents the results of the damage assessment test (SDT) and the material's
195 mechanical properties which are summarized in Table 4.

196 The slump and air content of fresh concrete were 155 mm [6.10 in] and 1.7% for sound concrete
197 mix and 155 mm [6.10 in] and 1.6% for ASR reactive concrete mix (CSA A23.2⁴¹).

198 The compressive strengths, f'_c , of sound concrete determined on cylinders at 7 and 28 days were
199 respectively 29.1 MPa (4220 psi) and 37.0 MPa (5370 psi), while compressive strengths of 29.8
200 MPa (4320 psi) and 36.3 MPa (5260 psi) were respectively measured for ASR reactive
201 concretes³⁶. It must be noted, however, that after 28 days of moist curing, none of the “reactive”
202 specimens showed macroscopic signs of ASR damage.

203 The steel reinforcing bars were tested in uniaxial tension in accordance with ASTM-E8⁴² and
204 ASTM-E111⁴³. The yield strength (f_y), the ultimate strength (f_u), the strain at rupture (ϵ_u) and the
205 Young's modulus (E_s) were respectively 456 MPa (66.1 ksi), 567 MPa (82.2 ksi), 0.175 and 190
206 GPa (27600 ksi).

207 **Observation of ASR Damage**

208 Observation of concrete cores extracted from specimen types A and D and examined with a
209 stereomicroscope (15X magnification) has revealed signs of damage associated with ASR which
210 may be characterized as follows: opened cracks in the coarse aggregate particles with reaction
211 product (OAC+RP), cracking in the cement paste with reaction product (CCP+RP), air voids
212 filled with reaction product (V+RP) and reaction rims around the reactive aggregate particles
213 (RR). These signs are typical of ASR and confirmed its presence in specimens A and D. In
214 addition, the reaction product observed in cracks and voids had the typical texture of alkali-silica
215 gel. Typical damage observed from polished concrete core sections are shown in Fig. 4 from a
216 specimen type A.

217 **Expansion**

218 Expansion was monitored in all three directions⁴⁴ but results are reported according to the highest

219 values measured, i.e. in the direction perpendicular to the casting plane, ε_p . Fig. 5 presents the
220 development of ε_p with time of conditioning for sound and ASR affected concrete blocks. The
221 shaded areas in the graphs mark the maximum and minimum expansion values. As noted in Fig. 5,
222 the conditioning period for the first and second series was about 100 and 200 days, respectively.
223 According to the rate of expansion, the ASR reaction seems to be constant during the first 200
224 days of conditioning. The average expansion reached for specimens A1 and A2 was respectively
225 0.20% and 0.33%, that corresponding to a severe and a very severe level of expansion and
226 concrete damage according to Sanchez & al.⁴⁵. For a severe level of expansion, cracks are
227 expected within and around the aggregates, and they are typically connected to other cracks for a
228 very severe level of expansion ⁴⁵. It can be seen that specimens type S did not experience
229 significant concrete expansion at 100 and 200 days. These results confirm the efficiency of the
230 added lithium nitrate solution into specimen S concrete mix for the duration of the project. After
231 the first and second series, specimens D1 and D2 were returned to conditioning for an additional
232 100 days. The average expansions before conditioning for the two specimens D1 and D2 were
233 0.21% and 0.32%. After the additional 100 days, the average expansion of specimens D1 and D2
234 was respectively 0.40% and 0.41%, that corresponding to a very severe level of expansion and
235 concrete damage⁴⁵.

236 The anisotropy of the reaction can be observed by comparing the expansions in parallel (ε_a) and
237 perpendicular (ε_p) directions to the casting plane (A-B and C-D axis in Fig. 2). As mentioned by
238 Smaoui & al.⁴⁶, the concrete expansion is highly related to the casting direction and the vibration
239 during the concrete placement. Fig. 6 compares ε_p and ε_a measured at the day of the test. It can be
240 seen that the expansion in the parallel direction is about 0.6 times the expansion in the
241 perpendicular direction (Eq. (1)). This figure also shows a good correlation between both the
242 expansions ε_p and ε_a (coefficient of determination $R^2 = 0.98$, coefficient of variation $CoV = 16\%$)

243 for ASR reactive specimens and a similar ratio was observed by Smaoui & al.⁴⁶.

244
$$\varepsilon_a = 0.601\varepsilon_p - 0.008 \quad (1)$$

245 where ε_p and ε_a are expressed in percentage.

246 **Material Properties**

247 The relation between ε_p and the mechanical properties of concrete cores extracted from tested
248 specimens are presented in Fig. 7. One can observe in Fig. 7a a significant decrease of the
249 compressive strength with increasing concrete expansion. By comparing the specimens S1 to A1
250 (approximately 100 days of conditioning), the compressive strength experienced a decrease of
251 19% (40.5 MPa [5870 psi] to 32.7 MPa [4740 psi] in average) with an expansion (ε_p) increase
252 from 0 to 0.20%. A similar behavior can be observed for the specimens S2 to A2
253 (approximately 200 days of conditioning) that experienced a decrease of their compressive
254 strength by about 31% (42.7 to 29.3 MPa in average) with an expansion (ε_p) increases from 0 to
255 0.33%. Interestingly, for a similar 35 MPa (5000 psi) concrete mix incorporating the same NM
256 aggregate, Sanchez & al.²² reported a 23% decrease in compressive strength for concrete cylinders
257 having reached an expansion of about 0.20%.

258 Compared to the concrete compressive strength, a less significant decrease of the splitting tensile
259 strength (f_{sp}) is observed in Fig. 7b and Table 4. While the tensile strength decreased between an
260 expansion of 0 and 0.20% (approximately 100 days of conditioning), no reduction of tensile
261 strength was measured afterward. Comparing the tensile strength of specimens S1 and A1, a
262 reduction of approximately 21% is found while a loss of 28% was observed looking at
263 specimens S2 and A2 (2.9 to 2.3 MPa [420 psi to 330 psi] and 3.1 to 2.2 MPa [450 psi to 320 psi]
264 respectively). As mentioned, the decrease of the tensile strength seems to have reached a plateau
265 from 0.20% to 0.41% of expansion. The reduction in tensile strength is actually very much related
266 to the type of testing method used⁴⁷. For instance, for a similar 35 MPa (5000 psi) concrete mix
267 incorporating the same NM aggregate, Sanchez & al.²² reported a 60% decrease in tensile strength

268 measured on concrete cylinders having reached an expansion of about 0.20% when using a gas
269 pressure tension test proposed by Komar & al.⁴⁸.

270 **Stiffness Damage Test**

271 As expected, no significant variation of Young's modulus of specimens S (around $\varepsilon_p = 0$) is
272 reported in Fig. 7c and Table 5. However, a significant decrease, of about 43% of Young's
273 modulus, was observed with an expansion ranging from 0.00 to 0.20% (35.2 to 19.2 GPa [5100 to
274 2780 ksi] on average). The decrease was less significant with an expansion progressing from
275 0.20% to 0.33%, and seemed to reach a plateau of about 15 GPa (2180 ksi) afterward. A similar
276 reduction of the Young's modulus (from 30 to 20 GPa [4350 to 2900 ksi]) was observed from 0 to
277 0.20% of expansion for the same concrete mix design tested by Sanchez & al.²². By comparing
278 the different parameters in Fig. 7, it can be seen that the Young's modulus results exhibit a smaller
279 scatter than results relative to compressive and tensile strengths for each series. This tends to
280 indicate that Young's modulus seems to be a better indicator of concrete expansion and therefore
281 of concrete damage than the other investigated mechanical properties (f'_c and f_{sp}).

282 Sanchez & al.²² carried-out SDT tests on twenty (20) different reactive aggregates and obtained
283 SDI values between 0.20 and 0.35 for a ASR expansion of 0.23% to 0.37% and between 0.23 to
284 0.37 for a ASR expansion of 0.30%, which agree well with the results presented in 8d. Indeed, the
285 average SDI of 0.12 and 0.09 was determined for specimens S1 and S2 (about no expansion)
286 respectively, while it was 0.27 and 0.33 for specimens A1 and A2 (average expansion of 0.20%
287 and 0.33%), respectively. Among the tested aggregates, NM coarse aggregates tested by Sanchez
288 & al.²² in cast concrete cylinder resulted in slightly lower SDI than the one presented in this
289 research. However, they agree well with the ones presented by Allard & al.⁴⁰ and obtained from
290 concrete cores extracted into affected concrete thick slab strips containing NM coarse aggregates.
291 Specimens D1 and D2 also presented in Table 4 experienced an average concrete expansion of
292 0.40% and 0.41%, respectively, and an average SDI of 0.31 and 0.37. For comparison, the average

293 SDI of specimens A2 (expansion of 0.33%) was 0.33. It therefore appears that increasing the
294 concrete expansion over 0.33% does not significantly affect the SDI of the NM aggregates. That
295 plateau was also observed by Sanchez²⁹ and Allard & *al.*⁴⁰ and was explained by the formation of
296 alkali-silica gel inside cracks, which mitigates the increase of SDI values with the increase of
297 ASR expansion.

298 **PULLOUT TEST RESULTS AND DISCUSSION**

299 The pullout tests results are presented in the following text and figures. A summary of the results
300 as well as measured embedded lengths are presented in Tables 4 and 5.

301 **Failure Mode**

302 Typical failure modes obtained for embedded lengths of $2d_b$, $4d_b$ and $5d_b$ are shown in Fig. 8 and
303 are summarized in Table 5. All specimens with a $2d_b$ embedded length failed after bar debonding
304 (failure mode D). Most of the specimens with a $4d_b$ embedded length failed by debonding after the
305 yielding of the bar (failure mode YD) while a few debonded just before yielding of the bar (mode
306 D). Specimens with a $5d_b$ embedded length having ASR reactive concrete also failed according to
307 the YD failure mode while they failed by bar rupture (mode U) for specimens with sound
308 concrete. Fig. 8 shows that some epoxy adhesive remained fixed between the bar ribs and that no
309 significant concrete material remained bonded to the epoxy adhesive (failure modes D and YD).
310 Consequently, the observe failure surface for pullout failure is located between the epoxy and the
311 concrete interface or through the adhesive, mainly along the bar ribs top surface.

312 **Bond-Slip Relationship**

313 Fig. 9 shows the bond stress, τ_b , according to the loaded end slip, s , of the post-installed
314 reinforcing bars. Fig. 9a, b and c respectively show the pullout results of specimens with
315 embedded length $2d_b$, $4d_b$ and $5d_b$ from first series and Fig. 9d, e and f, results from the second
316 series. The bond stress was determined by the force induced to the reinforcing bar for a specific
317 embedded length divided by the nominal surface area associated to that embedded length. The

318 embedded lengths presented in Table 5 were used to calculate bond stresses. Pullout energies, E ,
319 shown in Table 5 were calculated considering the area under the pullout curves from Fig. 9 for
320 slips ranging from 0 to 9.7 mm (0.382 in), i.e., the spacing between ribs for the reinforcing bars
321 used in this project (pitch).

322 As observed in Fig. 9 for specimens failing by debonding (Table 5), the bars experienced almost
323 no slip and have a large stiffness up to about 20 MPa (2900 psi), and then the bonded bar stiffness
324 decreases until the maximum bond stress is reached. Thereafter, except for specimens S1- $5d_b$ and
325 S2- $5d_b$ experiencing failure mode U (Fig. 9c and f), the bond stress progressively decreases until
326 complete pullout of the bar. Very similar bond-slip response and bond strength were observed for
327 epoxy-bonded bars embedded in sound concrete^{5, 34, 49}.

328 The average bond strengths of specimens S1, S2, A1 and A2 with an embedded length of $2d_b$ were
329 respectively 32.1, 33.2, 31.6 and 31.3 MPa (4660, 4790, 4580, 4540 psi) (Table 5). The results
330 were respectively 31.1, 32.2, 29.1 and 30.6 MPa (4510, 4670, 4220 and 4440 psi) for an
331 embedded length of $4d_b$ and 26.6, 28.0, 25.5 and 25.9 MPa (3860, 4060, 3700 and 3760 psi) for
332 embedded length $5d_b$. One can observe that the results between $2d_b$ and $4d_b$ specimens were
333 similar and that the ones with embedded length $5d_b$ experienced lower average bond strengths.
334 These results may be due to a non-uniform stress distribution along the bar for embedded length
335 longer than $4d_b$ [10]. Reinforcing bars embedded in sound concrete (A1 and A2) experienced
336 slightly higher bond strength and generally higher pullout energy than the ones embedded in
337 concrete affected by ASR (S1 and S2). Based on the pullout energy presented in Table 5, failures
338 of specimens S were generally less brittle (higher pullout energy) than the one of specimens A.
339 Moreover, specimen A1- $4d_b$ -2 exhibited a more brittle (lower pullout energy as shown on Table 5,
340 Fig 8 b) compared to the other tested A1- $4d_b$ specimens. Based on these results, the pullout
341 behavior of specimens with an embedded length of $4d_b$ embedded in ASR affected concrete seems

342 to be more variable than the one in sound concrete, considering that the specimen might
343 experience a more brittle failure.

344 Fig. 10 shows the relation between the bond strength and the concrete expansion for specimens
345 experiencing Y or YD failure modes from the first and second series (A1, A2, S1 and S2). As
346 previously mentioned, it can be seen that the bond strength slightly decreases with an increase of
347 the concrete expansion (approximately a 2 MPa decrease in average over the 0 to 0.33%
348 expansion range). It can also be observed that the bond strength of the specimens A1 and A2
349 spreads over a larger range than specimens S1 and S2 with sound concrete. The linear regression
350 between the bond strength and the concrete expansion for specimens experiencing Y or YD
351 failure modes is define by Eq. (2) (Predicted/Test = 1.01 and CoV = 10%).

$$352 \quad \tau_b = -4.83\varepsilon_p + 30.9 \text{ [MPa]} \quad (2)$$

353 where ε_p is expressed in percentage and, for customary units (psi), -4.83 and 30.9 have to be
354 replaced by 701 and 4482, respectively. From this equation, the development length of the tested
355 bars ($f_y = 456$ MPa, 66.1 ksi) is 59 mm (2.32 in) in sound concrete. In ASR affected concrete with
356 $\varepsilon_p = 0.33\%$, this development length increased to 62 mm (2.44 in).

357 Fig. 11 shows the bond stress due to the loaded end slip for specimens D1 and D2. As illustrated,
358 the average bond strengths of specimens D1- $4d_b$ and D2- $4d_b$ were respectively 30.3 and 32.0 MPa
359 (4390 and 4640 psi) compared to 29.1 and 30.6 MPa (4220 and 4440 psi) for specimens A1- $4d_b$
360 and A2- $4d_b$ (Table 5). Despite the progression of ASR following the bar installation on specimens
361 D, their average bond strength was slightly higher than the one of associated specimens A (no
362 progression of ASR after the installation of anchorage in specimens A). Progression of ASR
363 following the bar installation (specimens D) therefore increases the bond strength and requires
364 more pullout energy. According to the expansion results presented in Table 4, this increase could
365 be due to the expansion of the concrete caused by ASR which, in turn, produces a confinement

366 pressure around the bar. It has been reported that confinement pressure applied perpendicularly to
367 the bar axis has a significant effect on the bond strength^{19, 49, 50}. More energy is therefore required
368 to perform the bar pullout. However, similarly to the specimen A1-4 d_b -2, it can be observed that
369 the specimen D1-4 d_b -1 from the third series experienced a more brittle failure (lower pullout
370 energy as shown on Table 4) at bond strength of 27.9 MPa (4050 psi). It is suggested that the
371 scatter of these results may be due to the likelihood of encountering a crack in the embedment
372 length of the bar. The potential presence of cracks in the periphery of the bar reduces the area
373 available for the transfer of forces between the epoxy resin and the concrete matrix, causing a
374 drop in the mechanical capacity of the post-installed reinforcing bar.

375 Fig. 12 shows the relationship between the bond strength and the bar embedded length (h_{eff}) for
376 specimens from the first and the second series failing in to D and YD modes. For specimens of
377 sound concrete, no significant decrease of the bond strength is observed between embedded length
378 $2d_b$ and $4d_b$, and a lower bond strength for an embedded length $5d_b$. For ASR affected concrete
379 specimens, Fig. 12a shows that the effect of ASR on bond strength becomes significant for
380 embedded lengths greater than $4d_b$. One can observe that specimens A1- $5d_b$ and A2- $5d_b$ failed by
381 debonding (mode YD) while specimens S1- $5d_b$ and S2- $5d_b$ experienced bar rupture (mode U).
382 ASR affected concrete to reduce the bond strength of post-installed bonded bars of embedded
383 length $5d_b$. These results can be attributed to the higher probability to encounter a crack along a
384 longer post-installed reinforcing bar embedment interface.

385 Fig. 13 presents the relationship between the bond strength of specimens A and S with embedded
386 lengths $2d_b$ and $4d_b$ and parameters used to assess ASR damage, i.e., the concrete compressive
387 strength, the Young's modulus and the SDI. As shown in Fig. 13 specimens A experienced a
388 lower compressive strength, a lower Young's modulus and a higher SDI than comparison
389 specimens S. These results are associated with slightly lower bond strength. According to the

390 experimental results, relations between the bond strength and material characterization parameters
391 can be expressed as: Eq. (3), (4) and (5).

$$392 \quad \tau_b = 0.071f'_c + 29.3 \text{ [MPa]} \quad (3)$$

$$393 \quad \tau_b = \frac{E_c}{19500} + 30.5 \text{ [MPa]} \quad (4)$$

$$394 \quad \tau_b = -5.32SDI + 33.0 \text{ [MPa]} \quad (5)$$

395 For customary units (psi), 29.3, 30.5, 5.32 and 33.0 have to be replaced by 4250, 4420, 770 and
396 4790, respectively. Fig. 13 shows that the data dispersion expressed by the 95% confidence
397 interval and the coefficient of variation is narrower for the SDI results. Fig. 13c shows that the
398 SDI (CoV = 2.9%) seems to be a slightly more accurate parameter than the compressive strength
399 and the Young's modulus (Fig. 13a and b, both CoV = 3.1%) to assess the bond strength losses
400 associated with ASR damage.

401 The relation between the bond strength τ_b and the axial bar stress $f_{s, max}$ is presented in Fig. 14 for
402 specimens from the first and the second series failing according to modes D and YD. For
403 specimens A and S, the coefficients of determination, R^2 , between τ_b and $f_{s, max}$ are respectively
404 0.005 and 0.013. These coefficients reveal no relation between these two parameters. According
405 to these results, the effect of the transverse bar contraction due to the longitudinal bar tensile strain
406 has no influence on the bond strength of epoxy bonded bars experiencing a YD failure mode (Fig.
407 14a). For comparison purposes, this effect plays a major role for cast-in-place embedded bar in
408 concrete where the bond strength may be reduced up to about 75% after the yielding of the bar¹⁹,
409 ⁵¹. For cast-in-place bars, a large part of the bond strength can be attributed to the bearing action
410 of the bars ribs on the concrete. Contraction of the bar due to axial tension stress therefore reduces
411 the bearing area and the bond strength^{5, 52}. For post-installed bonded bars, it may be suggested
412 that the larger flexibility of the epoxy compared to the concrete ($E_b/E_c \sim 20$) may enable the

413 adhesive to follow the steel deformations and insure adequate bearing conditions for the bar ribs.
414 More studies are required to better understand this phenomenon.

415 **CONCLUSIONS**

416 The objectives of this research project were to investigate the effects of ASR deleterious
417 mechanisms on the bond strength of post-installed reinforcing bars and the effects of the
418 damaging ASR progression on bond strength after the embedment of the epoxy bonded bars.
419 According to the material investigation, the main conclusions are:

- 420 • Concrete expansion was measured both perpendicularly and parallel to the casting plane
421 during conditioning. A fairly strong anisotropy of the expansion was observed for
422 specimens affected by alkali-silica reaction (ASR) where the expansion in the parallel
423 direction was about 0.6 times the expansion in the perpendicular direction. The measured
424 concrete expansions corresponded to a severe or a very severe level of concrete damage.
- 425 • Compressive strength, tensile strength and Young's modulus have decreased with the
426 increasing of the ASR expansion. Both the tensile strength and the Young's modulus reach
427 a plateau for expansions exceeding 0.20%. The Young's modulus was the most affected
428 concrete mechanical property due to ASR.
- 429 • The stiffness damage index (SDI) values determined from the SDT were similar to the
430 results presented by Allard & *al.*⁴⁰ for NM coarse aggregate and have demonstrated that
431 the monitored concrete expansions are correlated to the damage state of ASR.

432 According to the investigation of ASR effects on the bonding behavior, the main conclusions are:

- 433 • Debonding failures were observed for specimens with $2d_b$ (bar diameter) embedded
434 length. Most of the specimens with $4d_b$ embedded lengths and ASR affected specimens
435 with $5d_b$ embedded lengths experienced debonding failures after yielding of the steel bar.
436 For these specimens, no significant concrete material remained bonded to the pulled out

437 bar. Finally, sound specimens with $5d_b$ embedded lengths experienced bar rupture.

438 • Pullout tests on epoxy bonded bars embedded in sound concrete and ASR affected
439 concrete have shown that ASR has not a large influence on bond strength although a
440 reduction of bond strength was observed for specimens affected by ASR.

441 • It was suggested that the decrease of the bond strength was caused by the presence of
442 longitudinal cracks (parallel to the bar axis) in the periphery of the bar. No significant
443 decrease of the bond strength was observed after the yielding of the epoxy bonded bars.

444 • SDI appeared to be the most accurate parameter to predict the bond strength of ASR
445 affected concrete and reduction of the bond strength prediction according to the SDI may
446 be a valuable avenue.

447 • The study revealed that the ASR progression after the embedment of reinforcing bars leads
448 to a confinement effect on the epoxy bonded bar which increased bond strength.

449 The proposed equations should be validated with more data and tests carried out with different
450 concrete strengths and ASR damage.

451 **ACKNOWLEDGMENTS**

452 The authors wish to express their gratitude and sincere appreciation to the Natural Sciences and
453 Engineering Research Council of Canada (NSERC), to the CREATE-INFRA program and to the
454 Research Center on Concrete Infrastructure (CRIB) for financing this research work and for
455 supporting several on-going related research projects.

456

NOTATION

457

458 A_b = reinforcing bar cross section area of

459 d_b = reinforcing bar diameter

460 F_R = rib index of reinforcing bar

461 E = pullout energy

462 E_b = Young's modulus of epoxy adhesive

463 E_c = Young's modulus of concrete

464 E_s = Young's modulus of reinforcing bar

465 f'_c = compressive strength of concrete

466 f_{sp} = tensile strength of concrete

467 f_s = axial reinforcing bar stress

468 f_y = yield strength of reinforcing bar

469 f_u = ultimate strength of reinforcing bar

470 h_{eff} = embedded length

471 s = relative displacement between concrete and reinforcing bar at the unloaded end (slip)

472 ε_p = expansion perpendicular to the concrete casting plane

473 ε_a = expansion parallel to the concrete casting plane

474 ε_u = strain at reinforcing bar rupture

475 τ = bond stress

476 τ_b = bond strength

477

478

REFERENCES

- 479 1. Mitchell D., Marchand J., Croteau P., Cook W. D., "Concorde Overpass Collapse: Structural Aspects",
480 *Journal of Performance of Constructed Facilities*, V. 25, No. 6, 2011, pp. 545-553.
- 481 2. Cusson B., "Renforcement des dalles épaisses en cisaillement", Québec, Canada: Université Laval; 2012,
482 143 pp.
- 483 3. Provencher P., "Renforcement des dalles épaisses en cisaillement", Québec, Canada: Université Laval; 2010,
484 130 pp.
- 485 4. Fernández Ruiz M., Muttoni A., Kunz J., "Strengthening of Flat Slabs Against Punching Shear Using Post-
486 Installed Shear Reinforcement", *ACI Structural Journal*, V. 107, No. 4, 2010, pp. 434-442.
- 487 5. Mahrenholtz C., "Seismic bond model for concrete reinforcement and the application to column-to-
488 foundation connections", Germany: University of Stuttgart; 2012, 417 pp.
- 489 6. Walraven J. C., "Aggregate interlock: a theoretical and experimental analysis", Netherlands: Delft
490 University; 1980, 210 pp.
- 491 7. Vecchio F. J., Collins M. P., "The modified compression-field theory for reinforced concrete elements
492 subjected to shear", *ACI Journal*, V. 83, No. 2, 1986, pp. 219-231.
- 493 8. Lutz L. A., Gergely P., "Mechanics of Bond and Slip of Deformed Bars in Concrete", *ACI Journal*
494 *Proceedings*, V. 64, No. 11, 1967, pp. 711-722.
- 495 9. ACI-408, "Bond and Development of Straight Reinforcing Bars in Tension", USA: American Concrete
496 Institute; 2003, 49 pp.
- 497 10. Azizinamini A., Chisala M., Ghosh S., "Tension development length of reinforcing bars embedded in high-
498 strength concrete", *Engineering Structures*, V. 17, No. 7, 1995, pp. 512-522.
- 499 11. Darwin D., Graham E. K., "Effect of Deformation Height and Spacing on Bond Strength of Reinforcing
500 bars", Lawrence, Kansas, USA: University of Kansas Center for Research; 1993, 71 pp.
- 501 12. Darwin D., Tholen M. L., Idun E. K., Zuo J., "Splice strength of high relative rib area reinforcing bars",
502 University of Kansas Center for Research, Inc.; 1995, 58 pp.
- 503 13. Darwin D., Zuo J., Tholen M. L., Idun E. K., "Development length criteria for conventional and high relative
504 rib area reinforcing bars", University of Kansas Center for Research, Inc.; 1995, 70 pp.
- 505 14. Eligehausen R., Popov E. P., Bertero V. V., "Local bond stress-slip relationships of deformed bars under

- 506 generalized excitations", United States: University of California at Berkeley; 1983, 169 pp.
- 507 15. Tepfers R., "A theory of bond applied to overlapped tensile reinforcement splices for deformed bars",
508 Sweden: Chalmers University of Technology; 1973, 328 pp.
- 509 16. Eligehausen R., Mallée R., Silva J. F., "Anchorage in concrete construction", John Wiley & Sons; 2006, pp.
- 510 17. Zuo J., Darwin D., "Splice Strength of Conventional and High Relative Rib Area Bars in Normal and High-
511 Strength Concrete", *ACI Structural Journal*, V. 97, No. 4, July-August 2000, pp. 630-641.
- 512 18. Mazzarolo E., Scotta R., Berto L., Saetta A., "Long anchorage bond-slip formulation for modeling of rc
513 elements and joints", *Engineering Structures*, V. 34, 2012, pp. 330-341.
- 514 19. fib, "fib Model Code for Concrete Structures 2010", Lausanne, Switzerland: Ernst and Sohn; 2013, 653 pp.
- 515 20. Lindgård J., Andiç-Çakır Ö., Fernandes I., Rønning T. F., Thomas M. D., "Alkali-silica reactions (ASR):
516 literature review on parameters influencing laboratory performance testing", *Cement and Concrete Research*, V. 42,
517 No. 2, 2012, pp. 223-243.
- 518 21. Sims I., Poole A. B., "Alkali-Aggregate Reaction in Concrete: A World Review", CRC Press; 2017, 768 pp.
- 519 22. Sanchez L., Fournier B., Jolin M., Mitchell D., Bastien J., "Overall assessment of Alkali-Aggregate Reaction
520 (AAR) in concretes presenting different strengths and incorporating a wide range of reactive aggregate types and
521 natures", *Cement and Concrete Research*, V. 93, 2017, pp. 17-31.
- 522 23. Thomas M. D., Fournier B., Folliard K. J., "Alkali-aggregate reactivity (AAR) facts book", FHWA-HIF-13-
523 019, United States: Federal Highway Administration (FHWA); 2013, 212 pp.
- 524 24. Hobbs D. W., "Alkali-silica reaction in concrete", Thomas Telford Publishing; 1988, 183 pp.
- 525 25. Nixon P., Bollinghaus R., "The effect of alkali aggregate reaction on tensile and compressive strength of
526 concrete", *Durability of building materials*, V. 2, No. 3, 1985, pp. 243-248.
- 527 26. Kubo Y., Nakata M., "Effect of reactive aggregate on mechanical properties of concrete affected by alkali-
528 silica reaction", *Proceedings 14th ICAAR - International Conference on Alkali-Aggregate Reaction in Concrete*, May
529 20-25th 2012, Austin (Texas), United States,
- 530 27. Giaccio G., Zerbino R., Ponce J., Batic O. R., "Mechanical behavior of concretes damaged by alkali-silica
531 reaction", *Cement and Concrete Research*, V. 38, No. 7, 2008, pp. 993-1004.
- 532 28. ISE, "Structural effects of alkali-silica reaction", United Kingdom: The Institution of Structural Engineers;
533 1992, 48 pp.
- 534 29. Sanchez L., "Contribution to the assessment of damage in aging concrete infrastructures affected by alkali-

535 aggregate reaction", Québec, Canada: Université Laval; 2014, 377 pp.

536 30. Villeneuve V., "Détermination de l'endommagement du béton par méthode pétrographique quantitative ",
537 Québec, Canada: Université Laval; 2011, 366 pp.

538 31. Thomas M. D., Fournier B., Folliard K. J., Ideker J. H., Resendez Y., "The Use of Lithium to Prevent or
539 Mitigate Alkali-Silica Reactions in Concrete Pavements and Structures", FHWA-HRT-06-133, United States: Federal
540 Highway Administration (FHWA); 2006, 54 pp.

541 32. ASTM-A996/A996M, "Standard Specification for Rail-Steel and Axle-Steel Deformed Bars for Concrete
542 Reinforcement", A996/A996M-16, West Conshohocken, PA, USA: ASTM International; 2016, 5 pp.

543 33. Cook R. A., "Behavior of Chemically Bonded Anchors", *Journal of Structural Engineering*, V. 119, No. 9,
544 1993, pp. 2744-2762.

545 34. Appl J.-J., "Tragverhalten von Verbunddübeln unter Zugbelastung (Load bearing behaviour of bonded
546 anchors under tension loading)", Stuttgart, Germany: Universität Stuttgart; 2009, 276 pp.

547 35. Sanchez L. F. M., Fournier B., Jolin M., Bastien J., "Evaluation of the stiffness damage test (SDT) as a tool
548 for assessing damage in concrete due to ASR: Test loading and output responses for concretes incorporating fine or
549 coarse reactive aggregates", *Cement and Concrete Research*, V. 56, 2014, pp. 213-229.

550 36. ASTM-C1231, "Standard Practice for Use of Unbonded Caps in Determination of Compressive Strength of
551 Hardened Cylindrical Concrete Specimens", C1231-14, USA: ASTM International; 2014, 10 pp.

552 37. ASTM-C496, "Standard Test Method for Splitting Tensile Strength of Cylindrical Concrete Specimens",
553 ASTM-C496-17, USA: ASTM International; 2017, 10 pp.

554 38. ASTM-C469, "Standard Test Method for Static Modulus of Elasticity and Poisson's Ratio of Concrete in
555 Compression", ASTM-C469-14, USA: ASTM International; 2014, 10 pp.

556 39. Sanchez L., Fournier B., Jolin M., Bastien J., Mitchell D., "Practical use of the Stiffness Damage Test (SDT)
557 for assessing damage in concrete infrastructure affected by alkali-silica reaction", *Construction and Building
558 Materials*, V. 125, 2016, pp. 1178-1188.

559 40. Allard A., Bilodeau S., Pissot F., Fournier B., Bastien J., Bissonnette B., "Performance evaluation of thick
560 concrete slabs affected by alkali-silica reaction (ASR) : Part 1 : Material aspects", *Proceedings 15th International
561 Conference on Alkali-Aggregate Reaction*, 2016, São Paulo, Brazil, pp. 10.

562 41. A23.1-14/A23.2-14 C., "Concrete materials and methods of concrete construction / Test methods and
563 standard practices for concrete", CSA Group; 2014, 690 pp.

- 564 42. ASTM-E8, "Standard Test Methods for Tension Testing of Metallic Materials", ASTM-E8/E8M-13, USA:
565 ASTM International; 2013, 28 pp.
- 566 43. ASTM-E111, "Standard Test Method for Young's Modulus, Tangent Modulus, and Chord Modulus",
567 ASTM-E111-17, USA: ASTM International; 2017, 14 pp.
- 568 44. Villemure F.-A., "Effet de la réaction alcalis-silice (RAS) sur l'adhérence des ancrages époxydiques de
569 barres d'armature", Québec, Canada: Université Laval; 2018, 202 pp.
- 570 45. Sanchez L. F. M., Multon S., Sellier A., Cyr M., Fournier B., Jolin M., "Comparative study of a chemo-
571 mechanical modeling for alkali silica reaction (ASR) with experimental evidences", *Construction and Building*
572 *Materials*, V. 72, Dec 2014, pp. 301-315.
- 573 46. Smaoui N., Bérubé M.-A., Fournier B., Bissonnette B., "Influence of specimen geometry, orientation of
574 casting plane, and mode of concrete consolidation on expansion due to ASR", *Cement, Concrete & Aggregates*, V.
575 26, 2004, pp. 58-70.
- 576 47. Clayton N., Currie R., Moss R., "Effects of alkali-silica reaction on the strength of prestressed concrete
577 beams", *The Structural Engineer*, V. 68, No. 15, 1990, pp. 287-292.
- 578 48. Komar A., Hartell J., Boyd A., "Pressure tension test: reliability for assessing concrete deterioration",
579 *Proceedings Seventh International Conference on Concrete under Severe Conditions - Environment and Loading*,
580 2013, Nanjing, China,
- 581 49. Lowes L. N., Moehle J. P., Govindjee S., "Concrete-Steel Bond Model for Use in Finite Element Modeling
582 of Reinforced Concrete Structures", *ACI Structural Journal*, V. 101, No. 4, July-Aug 2004, pp. 501-511.
- 583 50. ACI Committee 408, "Bond and Development of Straight Reinforcing Bars in Tension", United States:
584 American Concrete Institute; 2003, pp.
- 585 51. Shima H., Chou L.-L., Okamura H., "Bond Characteristics in Post-Yield Range of Deformed Bars", *Doboku*
586 *Gakkai Ronbunshu*, V. 1987, No. 378, 1987, pp. 213-220.
- 587 52. Brantschen F., Faria D. M., Fernández Ruiz M., Muttoni A., "Bond behaviour of straight, hooked, U-shaped
588 and headed bars in cracked concrete", *Structural Concrete*, V. 17, No. 5, 2016, pp. 799-810.
- 589
- 590

591

TABLES AND FIGURES

592 **List of Tables:**

593 **Table 1** – Petrographic facies and potentially reactive phases of New Mexico aggregate from

594 Villeneuve (2011)

595 **Table 2** – Concrete mixes design (kg/m^3)

596 **Table 3** – Properties of the epoxy resin according the manufacturer

597 **Table 4** – Expansion and mechanical properties summary

598 **Table 5** – Pullout test results summary

599 **List of Figures:**

600 **Fig. 1** – a) Drilling in concrete, b) insertion of a bar into epoxy adhesive, c) shear strengthened RC

601 member with epoxy-bonded bars

602 **Fig. 2** – Orientation of the expansion measurement according to the casting plane

603 **Fig. 3** – Experimental setup for confined pullout test

604 **Fig. 4** – Typical damage caused by ASR

605 **Fig. 5** – Concrete expansion according to the number of days of conditioning

606 **Fig. 6** – Relationship between ε_a and ε_p

607 **Fig. 7** – Relationship between ε_p and (a) f'_c (b) f_{sp} (c) E_c (d) SDI

608 **Fig. 8** – Typical failures observed from unconfined pullout test

609 **Fig. 9** – Relationship between τ and s : (a) (b) (c) First series (S1, A1); (d) (e) (f) Second series

610 (S2, A2)

611 **Fig. 10** – Failure modes D and YD: Relationship between τ_b and ε_p

612 **Fig. 11** – Relationship between τ and s for the third series (D1, D2)

613 **Fig. 12** – Relationship between τ_b and h_{eff} for specimens of (a) ASR affected concrete (S1, S2) and

614 (b) sound concrete (A1, A2)

615 **Fig. 13** – Relationship between τ_b and (a) f'_c (b) E_c (c) SDI for embedded lengths of $2d_b$ and $4d_b$

616 **Fig. 14** – Failure modes D and YD: Relationship between τ_b and $f_{s, max}$ for specimens of (a) ASR

617 affected concrete (A1, A2) (b) sound concrete (S1, S2)

618

619

TABLES

620 *Table 1 – Petrographic facies and potentially reactive phases of New Mexico aggregate from*
 621 *Villeneuve (2011)*

<i>Facies</i>	<i>Type</i>	<i>Proportion [%]</i> <i>(-14 + 10 mm [-0.55 + 0.39 in])</i>	<i>Proportion [%]</i> <i>(-20 + 14 mm [-0.78 + 0.55 in])</i>	<i>Potentially reactive phases</i>
A	Andesite-basalt	19.0	36.1	Volcanic glass
B	Quartzite	56.7	35.4	Microcrystalline quartz (10%)
C	Granite	18.5	20.1	Microcrystalline quartz (5%) and quartz with undulatory extinction
D	Granitic gneiss	2.8	3.3	Quartz with undulatory extinction
E	Rhyolite	2.6	2.0	Microcrystalline quartz (~20%)
F	Pelite	0.4	3.1	-

622

623 *Table 2 – Concrete mixes design (kg/m³)*

<i>Components</i>	<i>ASR reactive concrete</i>	<i>Sound concrete</i>
Cement	370.0	370.0
Fine aggregate	742.6	742.6
Coarse aggregate	1091.8	1091.8
NaOH	0.7	-
Lithium nitrate (LiNO ₃)	-	28.3
Water	174.0	174.0
Density	2368	2376

624 Note: 1 kg/m³ = 1.686 lb/yd³

625

626 *Table 3 – Properties of the epoxy resin according the manufacturer*

Bond strength (ASTM C882-91)	12.4 MPa (1800 psi)
Compressive strength (ASTM D-695-96)	82.7 MPa (12000 psi)
Compressive modulus (ASTM D-695-96)	1493 MPa (220 ksi)
Tensile strength (ASTM D-638-97)	43.5 MPa (6310 psi)
Elongation at break (ASTM D-638-97)	2.0%

627

628 Table 4 – Expansion and mechanical properties summary

	Specimens	ε_p [%]	ε_a [%]	f'_c [MPa]	f_{sp} [MPa]	E_c [GPa]	SDI
First series	S1	-0.013	-0.017	40.5	2.9	35.3	0.12
	A1	0.198	0.111	32.7	2.3	19.1	0.27
Second series	S2	0.015	-0.004	42.7	3.1	35.1	0.10
	A2	0.327	0.185	29.3	2.2	16.0	0.33
Third series	D1	0.402	0.225	28.6	2.3	16.0	0.31
	D2	0.406	0.255	24.7	2.6	14.4	0.37

629 Note: 1 MPa = 0.001 GPa = 145.038 psi

630

631 Table 5 – Pullout test results summary

Specimen	Failure Mode	h_{eff} [mm]	$f_{s,max}$ [MPa]	τ_b [MPa]	E [J]		
S1-2 d_b -1	D	32.7	236	28.6	32.1	348	394
S1-2 d_b -2	D	32.4	261	32.1		379	
S1-2 d_b -3	D	34.0	287	33.6		437	
S1-2 d_b -4	D	30.9	263	34.0		410	
S1-4 d_b -1	YD	62.3	473	30.2	31.1	480	496
S1-4 d_b -2	YD	61.0	485	31.7		465	
S1-4 d_b -3	YD	67.0	540	32.1		544	
S1-4 d_b -4	YD	67.7	519	30.5		-	
S1-5 d_b -1	U	84.0	553	26.9	26.6	-	-
S1-5 d_b -2	U	86.2	582	26.3		-	
A1-2 d_b -1	D	32.6	260	31.7	31.6	230	344
A1-2 d_b -2	D	32.4	254	31.3		287	
A1-2 d_b -3	D	34.8	276	31.6		426	
A1-2 d_b -4	D	33.4	268	31.9		434	
A1-4 d_b -1	YD	68.9	527	30.6	29.1	485	427
A1-4 d_b -2	D	62.0	362	23.2		296	
A1-4 d_b -3	D	53.2	449	33.6		501	
A1-5 d_b -1	YD	87.4	564	25.7	25.5	441	432
A1-5 d_b -2	YD	86.2	559	25.8		434	
A1-5 d_b -3	YD	82.0	512	25.0		421	
S2-2 d_b -1	D	38.1	338	35.4	33.2	399	417
S2-2 d_b -2	D	35.1	286	32.4		395	
S2-2 d_b -3	D	32.6	266	32.5		420	
S2-2 d_b -4	D	32.9	268	32.4		455	
S2-4 d_b -1	YD	67.3	545	32.2	32.2	577	539
S2-4 d_b -2	YD	63.9	541	33.7		539	
S2-4 d_b -3	YD	63.5	519	32.5		540	
S2-4 d_b -4	YD	61.4	468	30.3		499	
S2-5 d_b -1	U	80.1	565	28.1	28.0	-	-
S2-5 d_b -2	U	80.8	565	27.8		-	
A2-2 d_b -1	D	31.8	252	31.8	31.3	360	366
A2-2 d_b -2	D	31.5	253	32.1		291	
A2-2 d_b -3	D	34.1	274	32.1		402	
A2-2 d_b -4	D	32.6	284	29.3		412	
A2-4 d_b -1	YD	62.4	476	30.4	30.6	423	435
A2-4 d_b -2	D	52.6	401	30.3		421	
A2-4 d_b -3	D	50.9	396	31.1		461	
A2-5 d_b -1	YD	81.4	533	26.0	25.9	441	462
A2-5 d_b -2	YD	82.4	535	25.8		482	
D1-4 d_b -1	D	65.3	457	27.9	30.3	363	460
D1-4 d_b -2	YD	65.3	537	32.7		557	
D2-4 d_b -1	YD	65.6	524	32.0	32.0	573	555
D2-4 d_b -2	YD	66.1	526	31.9		537	

632 Note: *anchor in a block tested twice, 1 mm = 0.03937 in, 1 MPa = 145.038 psi

Fig. 1

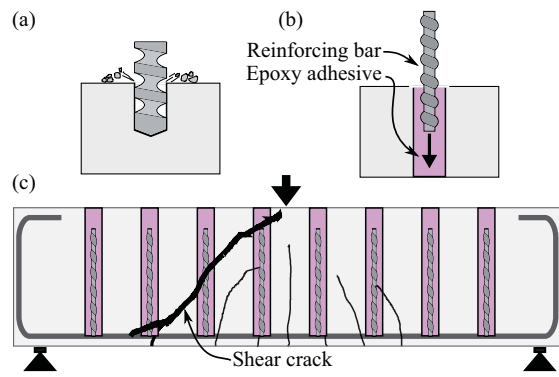


Fig. 2

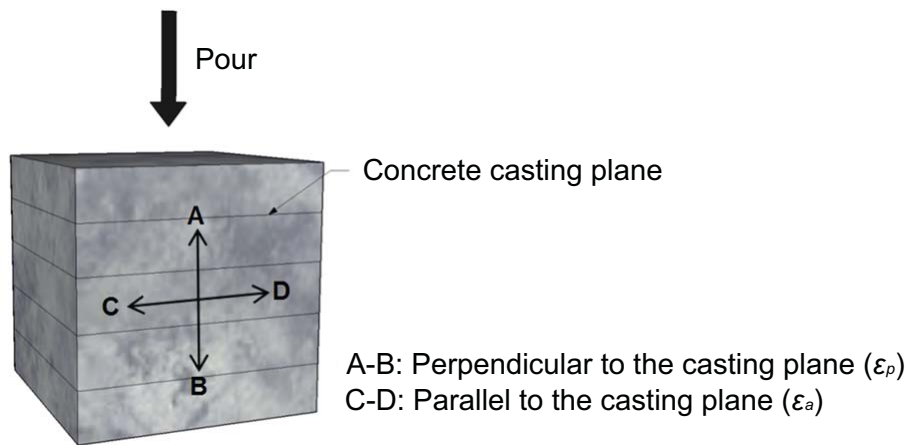


Fig. 3

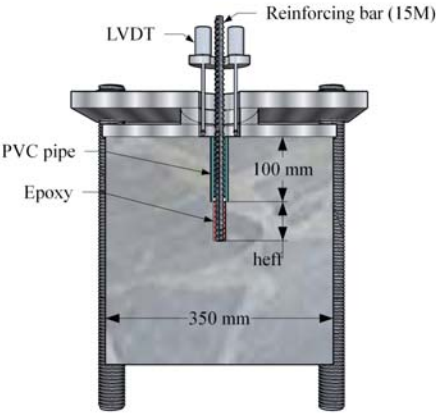


Fig. 4

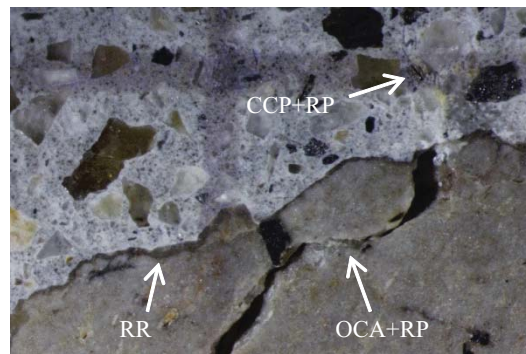


Fig. 5

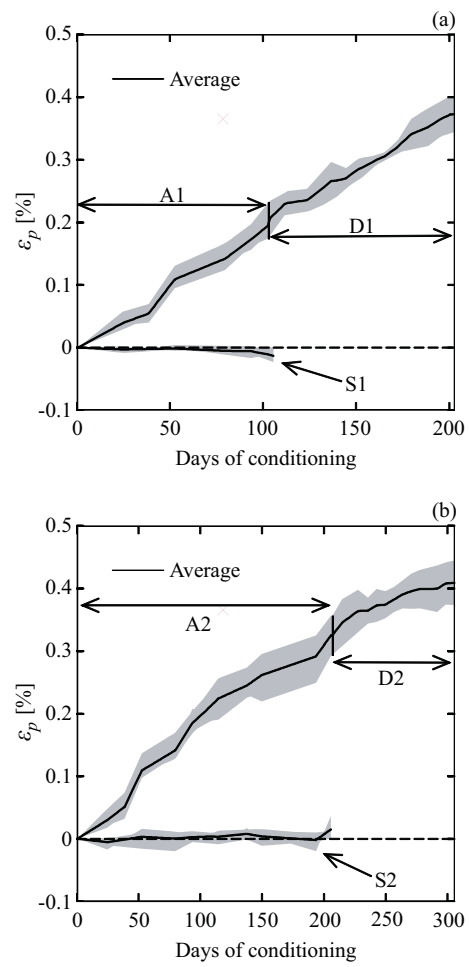


Fig. 6

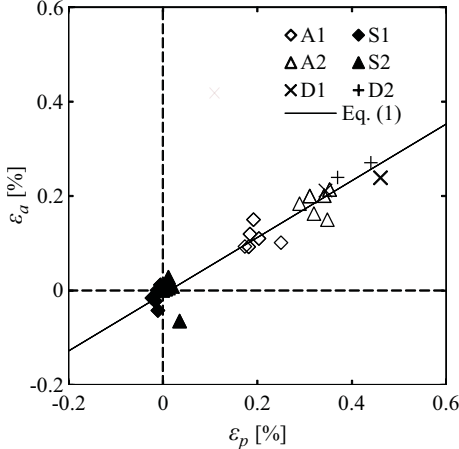


Fig. 7

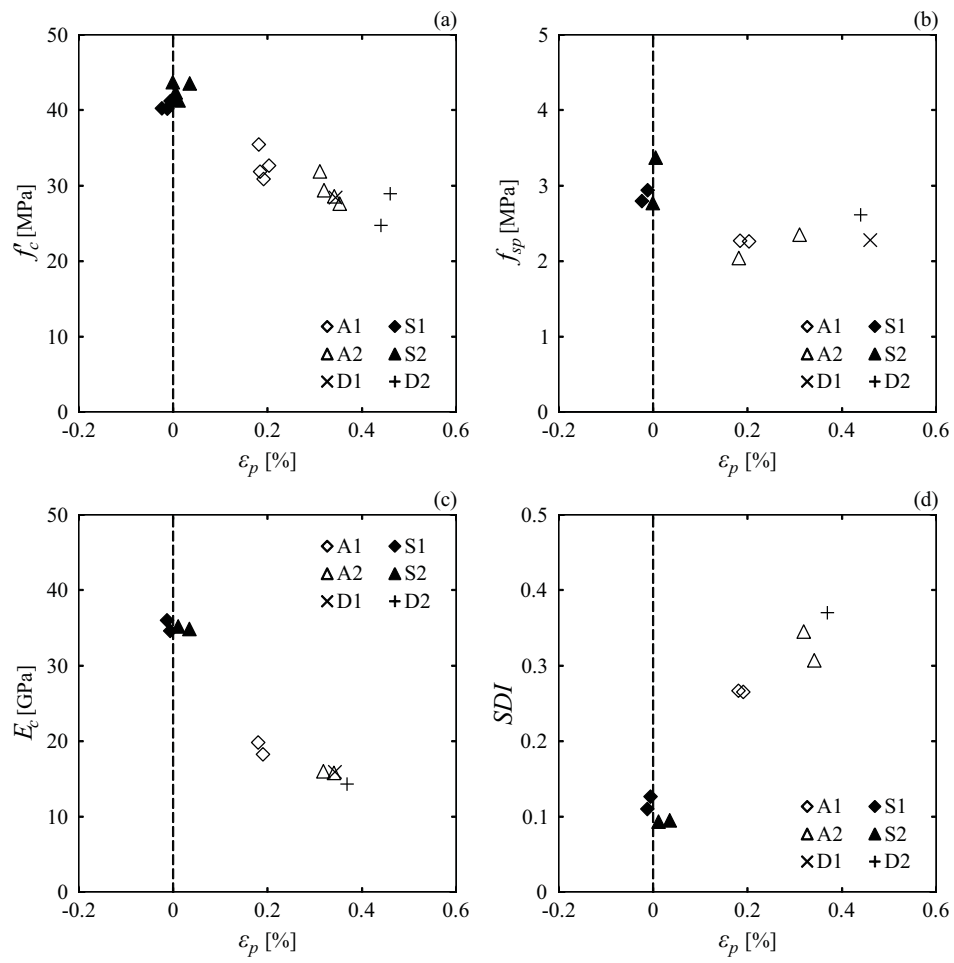


Fig. 8



Fig. 9

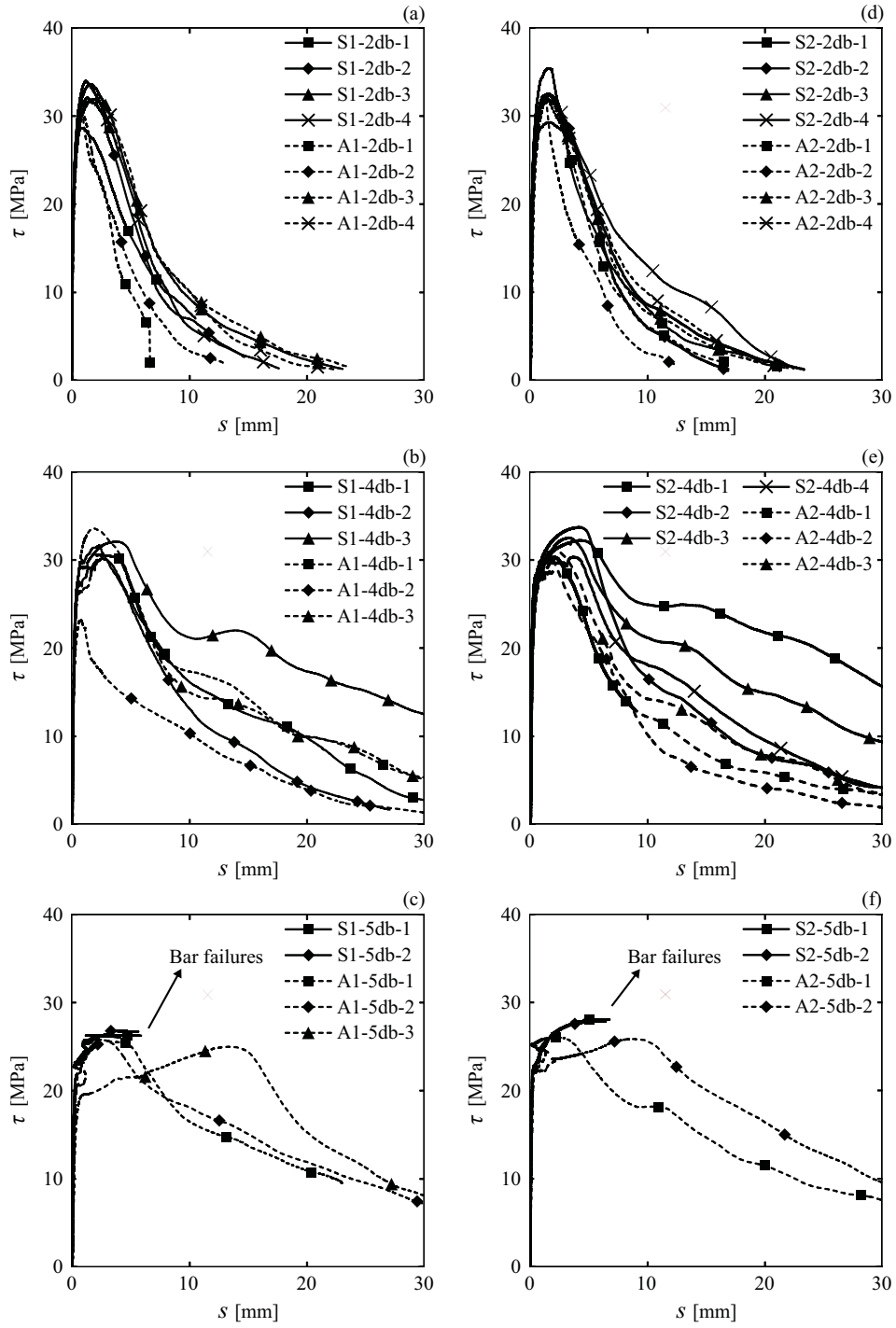


Fig. 10

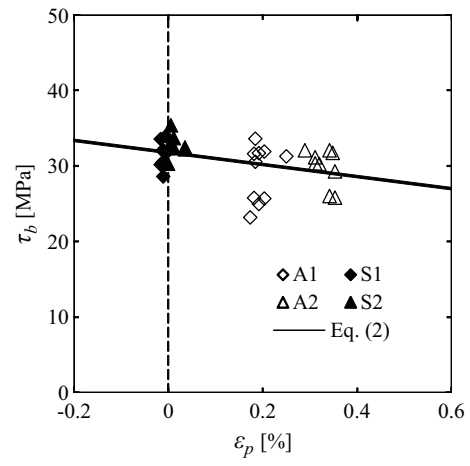


Fig. 11

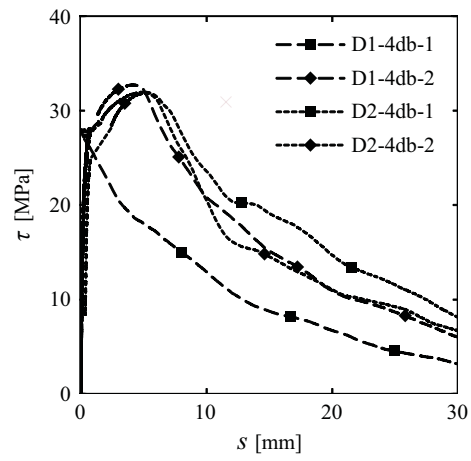


Fig. 12

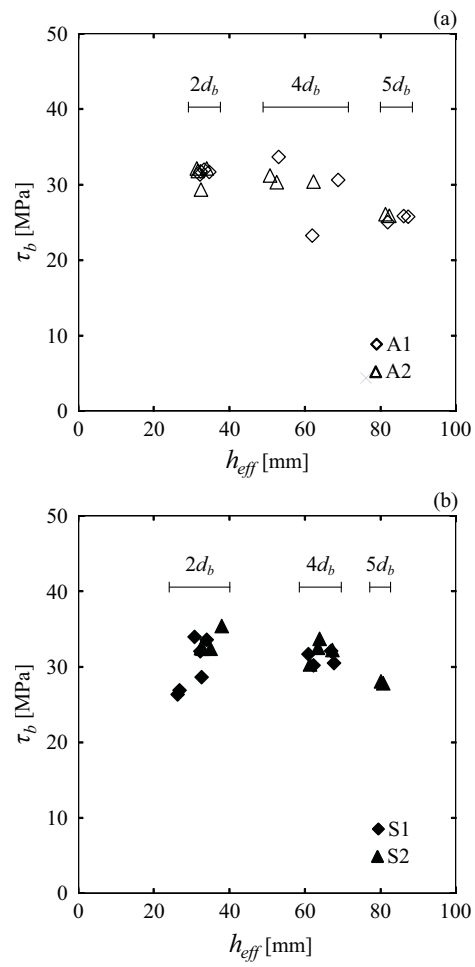


Fig. 13

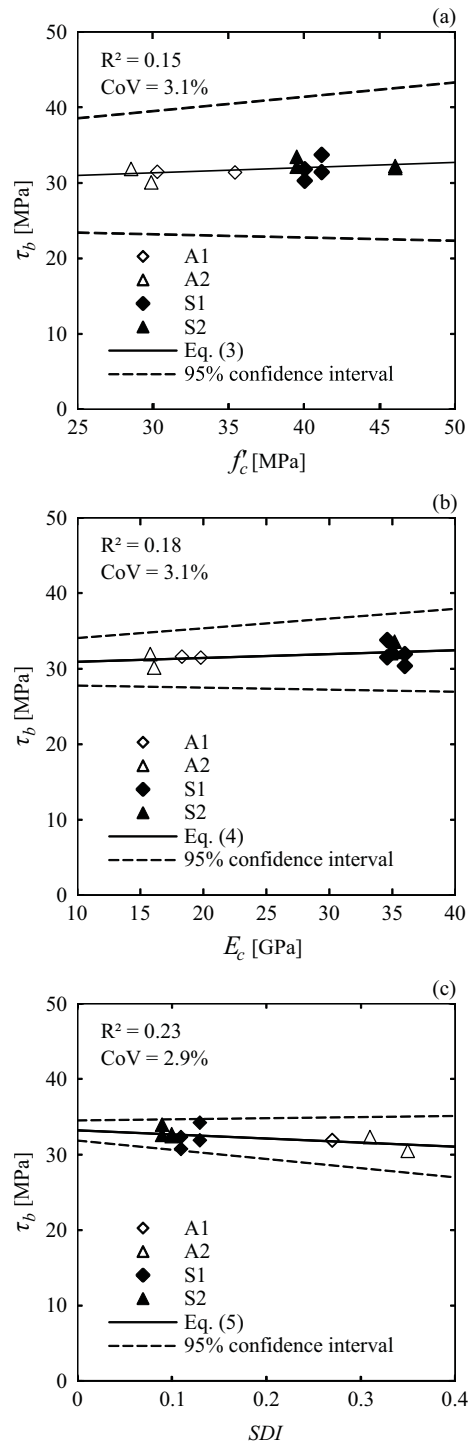


Fig. 14

